PHYSICAL REVIEW D VOLUME 44, NUMBER 9 1 NOVEMBER 1991

High-energy photons from quark-gluon plasma versus hot hadronic gas

Joseph Kapusta
School of Physics and Astronomy, University of Minnesota, Minneapolis, Minnesota 55455

Peter Lichard*
Theoretical Physics Institute, University of Minnesota, Minneapolis, Minnesota 55455

David Seibert†
School of Physics and Astronomy, University of Minnesota, Minneapolis, Minnesota 55455
(Received 3 June 1991)

Photons in the energy range of about one-half to several GeV have been proposed as a signal of the formation of a quark-gluon plasma in high-energy collisions. To lowest order the thermal emission rate is infrared divergent for massless quarks, but we regulate this divergence using the resummation technique of Braaten and Pisarski. Photons can also be produced in the hadron phase. We find that the dominant contribution comes from the reactions $\pi\pi \to \rho\gamma$ and $\pi\rho \to \pi\gamma$; the decays $\omega \to \pi\gamma$ and $\rho \to \pi\pi\gamma$ are also significant. Comparing the thermal emission rates at a temperature $T = 200$ MeV we conclude that the hadron gas shines just as brightly as the quark-gluon plasma.

I. INTRODUCTION

Formation and observation of a quark-gluon plasma in ultrarelativistic collisions between heavy nuclei is an important goal of modern nuclear physics. Experiments are now being carried out at Brookhaven's Alternate Gradiant Synchrotron (AGS) and at CERN's Super Proton Synchrotron (SPS), and in the future there will be experiments at Brookhaven's Relativistic Heavy Ion Collider (RHIC) and at CERN's Large Hadron Collider (LHC). The energies involved range from 14.5 GeV per nucleon in a fixed-target mode at the AGS to several TeV per nucleon in a colliding-beam mode with lead nuclei at the LHC. Even if a quasiequilibrated plasma is created for a brief time in these collisions it is still a challenge to infer knowledge of the plasma from particle distributions. In principle we would like to infer various correlation functions as probes of the dynamics of the plasma in the same way as correlation functions are studied in condensed-matter systems. Unfortunately we are at the mercy of nature because, unlike condensed-matter physicists, we cannot insert an external probe such as a thermometer or voltmeter. We are totally dependent upon whatever particles are thrown out of the collision.

Among the proposed "probes" of the plasma are the directly produced real photons [1–6]. These could come from the annihilation process $q\bar{q} \to g\gamma$ and from the QCD Compton process $qg \to q\gamma$, $\bar{q}g \to \bar{q}\gamma$. These photons interact only electromagnetically, unlike pions, and so their mean free paths are typically much larger than the transverse size of the region of hot matter created in any nuclear collision. As a result, high-energy photons produced in the interior of the plasma usually pass through the surrounding matter without interacting, carrying information directly from wherever they were formed to the detector. This makes them an interesting object of study to both theorists and experimenters.

In this paper we do not concern ourselves directly with the complicated dynamics of nuclear collisions at high energy. Instead we focus on simpler, but still difficult, questions: What is the spectral emissivity of quark-gluon plasma? What is the spectral emissivity of hot hadronic matter? How do they compare at the same temperature? These are important questions. Suppose we put a hadron gas in one box and a quark-gluon plasma in another, and maintain them at the same temperature T. Can we tell which box contains the quark-gluon plasma by looking through a small window and measuring the photon spectrum?

If we wait long enough the answer is clearly no. Even if we do not put any photons into the boxes at the beginning, matter will eventually come to equilibrium under the electromagnetic interactions. To a good approximation the final photon distribution will be just the Planck distribution at temperature T.

Fortunately, in conditions more appropriate to a nuclear collision the answer is yes. A closer analogue to a nuclear collision is to make the boxes smaller than the photon mean free path and to make the walls transparent to photons, so that the photons always escape and the photon distribution stays far from equilibrium. The spectral emissivity then directly reflects the dynamics of real photon producing reactions in the matter, which may be different for the two phases.

The thermal production rates in the two phases are important in another sense. Suppose that quark-gluon plasma is formed in a collision. It will expand and eventually hadronize in a (presumably first-order) phase transition. The hadrons themselves may maintain local thermal equilibrium for a while also producing photons. The

total yield is a sum of the yields from both phases.

In a nucleus-nucleus collision the primary background for photon production with transverse momentum less than 2 or 3 GeV are the decays $\pi^0 \to \gamma\gamma$, $\eta \to \gamma\gamma$; the decays of ω and η' would contribute a few percent more. Generally one might expect meson decays in the final state to be the dominant source of photons; however, there is a very real difference between the two sources. The number of photons contributed by meson decay scales with the total number of charged particles produced in the collision, whereas the number of photons produced by quark and gluon reactions would be expected to scale with the square of the number of charged particles [7]. Another way to think of it is that the number of photons contributed by the quark-gluon plasma is obtained by integrating the rate R (number of reactions per unit time per unit volume which produce a photon) over the space-time history of the collision. Roughly speaking, the yield is *rate* × *volume* × *time*. The yield from final-state meson decays is proportional to the volume. So, if the plasma "lives" a long time more photons will be produced.

In this paper we report the following accomplishments. In Sec. II we reconsider the QCD annihilation and Compton reactions to high-energy photon production ($E > 3T$). As is well known these rates are divergent in the limit of vanishingly small quark masses. For the first time we get an accurate assessment of these rates by implementing the infrared resummation technique of Braaten and Pisarski [8]. We find that this technique works beautifully, as it matches smoothly on to the rate based on the two-loop photon self-energy (equivalent in this context to relativistic kinetic theory). In Sec. III we compute the thermal rate in the hadron phase to the same order as it has been computed in the quark-gluon-plasma phase. The dominant reactions turn out to be the exact analogues of the QCD reactions, namely, annihilation $\pi\pi \to \rho\gamma$ and Compton $\pi\rho \to \pi\gamma$. Surprisingly, to our knowledge, no one has previously made any estimate of these rates in the hadron phase. We compare the rates in the two phases at $T = 200$ MeV in Sec. IV with a startling result. In Sec. V we estimate the effect of form factors on the rates computed in the hadron phase, and find them to be not very important up to photon energies of 2 GeV. Our conclusions are given in Sec. VI.

II. PHOTONS FROM QUARK-GLUON PLASMA

The thermal emission rate of photons with energy E and momentum $\mathbf{p}$ from a small system (compared to the photon mean free path) is

$$E\frac{dR}{d^3p} = \frac{-2}{(2\pi)^3}\,\mathrm{Im}\Pi^{R,\mu}_{\mu}\,\frac{1}{e^{E/T}-1}\ , \tag{1}$$

where $\Pi^R_{\mu\nu}$ is the retarded photon self-energy at finite T. This formula has been derived both perturbatively [9,10] and nonperturbatively [11]. It is valid to all orders in the strong interactions, but only to order e^2 in the electromagnetic interactions, as in the derivation it was assumed that the produced photons emerged from the matter without final-state scattering.

FIG. 1. One- and two-loop contributions to the photon self-energy in QCD.

If the photon self-energy is approximated by carrying out a loop expansion to some finite order then the formulation of Eq. (1) is equivalent to relativistic kinetic theory. Let $\mathcal{M}$ be the amplitude for a reaction m particles $\to$ n particles + one photon. The contribution of this reaction to the total rate R is

$$\mathcal{N}\int d\Phi\,(2\pi)^4\,\delta(p^\mu_{\rm in} - p^\mu_{\rm out})\,|\mathcal{M}|^2\ . \tag{2}$$

Here $d\Phi$ is the phase space: a factor $d^3p/2E(2\pi)^3$ for each particle and the photon, a Bose-Einstein or Fermi-Dirac distribution for each particle in the initial state, and a Bose-enhancement or Pauli-suppression factor for each particle in the final state. The overall degeneracy factor $\mathcal{N}$ depends on the specific reaction. Expanding the photon self-energy up to and including L loops is equivalent to computing the contribution from all reactions with $n+m \le L+1$, with each amplitude computed only to order g^{L-1}.

In Sec. II A the thermal rate is computed using the kinetic theory formalism for the QCD Compton and annihilation reactions. Because the quark masses m_u and m_d are set to zero, an infrared cutoff $-k_c^2$ must be placed on the four-momentum transfer. In Sec. II B the infrared divergence is regulated by an infinite resummation of finite-temperature Feynman diagrams following Braaten and Pisarski [8]. This amounts to a careful treatment of the small part of phase space left out of the kinetic theory calculation when the infrared cutoff is imposed. In Sec. II C we add the contributions from the two regions of phase space: the result is independent of the cutoff. The thermal QCD rate is thus well defined even for massless quarks.

A. QCD kinetic theory

The one- and two-loop contributions to $\Pi_{\mu\nu}$ are shown in Fig. 1. The imaginary part is obtained by cutting the diagrams. Cutting the one-loop diagram gives zero when the photon is on mass shell since $q\bar{q} \to \gamma$ has no phase

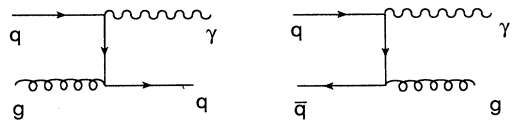

FIG. 2. QCD Compton and annihilation reactions for photon production arising from the imaginary parts of the two-loop diagrams in Fig. 1.

space. Certain cuts of the two-loop diagrams give order g^2 corrections to the nonexistent reaction $q\bar{q} \to \gamma$, while other cuts correspond to the reactions $q\bar{q} \to g\gamma$, $qg \to q\gamma$, and $\bar{q}g \to \bar{q}\gamma$ as shown in Fig. 2. Let $\mathcal{M}_i$ represent the amplitude for one of these. The contribution to the rate is

$$R_i = \mathcal{N} \int \frac{d^3p_1}{2E_1(2\pi)^3} \frac{d^3p_2}{2E_2(2\pi)^3} f_1(E_1) f_2(E_2) (2\pi)^4 \delta(p_1^\mu + p_2^\mu - p_3^\mu - p^\mu) \mid \mathcal{M}_i \mid^2 \frac{d^3p_3}{2E_3(2\pi)^3} \frac{d^3p}{2E(2\pi)^3} [1 \pm f_3(E_3)] \ , \tag{3}$$

where the f's are the Fermi-Dirac or Bose-Einstein distribution functions as appropriate, and there is either a Bose enhancement or Pauli suppression of the strongly interacting particle in the final state.

This rate can be simplified. Define $s = (p_1 + p_2)^2$ and $t = (p_1 - p)^2$. Insert integrations over s and t with a delta function for each of these identities. This is a natural thing to do because the invariant amplitude depends only on these two variables. Converting the total rate to a differential one, all but four of the integrations can be done without approximation:

$$E\frac{dR_i}{d^3p} = \frac{\mathcal{N}}{(2\pi)^7} \frac{1}{16E} \int ds\, dt \mid \mathcal{M}_i(s,t) \mid^2 \int dE_1\, dE_2\, f_1(E_1) f_2(E_2) \times [1 \pm f_3(E_1 + E_2 - E)] \theta(E_1 + E_2 - E)(aE_1^2 + bE_1 + c)^{-1/2} \ , \tag{4}$$

where

$$\begin{aligned} a &= -(s+t)^2 \ , \\ b &= 2(s+t)(Es - E_2 t) \ , \\ c &= st(s+t) - (Es + E_2 t)^2 . \end{aligned} \tag{5}$$

Presently we are interested in the case where the photon energy is large, $E_1 + E_2 > E \gg T$. In this limit it is a good approximation to replace

$$f_1(E_1) f_2(E_2) \to e^{-(E_1+E_2)/T} \ . \tag{6}$$

Even though E_1 or E_2 separately need not be large, phase space is unfavorable for it. Corrections to Eq. (6) should be suppressed when E is large compared to T. This approximation can be checked numerically (Sec. II C). Then the integrations over E_1 and E_2 can be done with the relatively simple result

$$E\frac{dR_i}{d^3p} = \frac{\mathcal{N}}{(2\pi)^6} \frac{T}{32E} e^{-E/T} \int \frac{ds}{s} \ln(1 \pm e^{-s/4ET})^{\pm 1} \times \int dt \mid \mathcal{M}_i(s,t) \mid^2 \ . \tag{7}$$

The upper sign is for particle 3 a fermion, the lower sign is for particle 3 a boson.

For massless particles the amplitude is related to the differential cross section by

$$\frac{d\sigma}{dt} = \frac{\mid \mathcal{M} \mid^2}{16\pi s^2} \ . \tag{8}$$

For the annihilation diagram

$$\frac{d\sigma}{dt} = \frac{8\pi\alpha\alpha_s}{9s^2} \frac{u^2 + t^2}{ut} \ , \tag{9}$$

and $\mathcal{N} = 20$ when summing over u and d quarks. For the Compton reaction

$$\frac{d\sigma}{dt} = \frac{-\pi\alpha\alpha_s}{3s^2} \frac{u^2 + s^2}{us} \ , \tag{10}$$

and $\mathcal{N} = \frac{320}{3}$. The integral over t just gives the total cross section. But, the total cross section involving the exchange of a massless particle is infinite. The differential cross sections have a pole at t and/or $u = 0$. Many-body effects are necessary to screen this divergence. We will show how this works in the next subsection. For now we delete that region of phase space causing the divergence. We integrate over

$$-s + k_c^2 \le t \le -k_c^2 \ , \tag{11}$$

$$2k_c^2 \le s < \infty \ , \tag{12}$$

where $T^2 \gg k_c^2 > 0$ is an infrared cutoff. This way of regulating the divergence treats u and t symmetrically and maintains the identity $s + t + u = 0$ appropriate for all massless particles.

In the limit that $k_c^2 \to 0$ we find

$$E\frac{dR^{\text{Compton}}}{d^3p} = \frac{5}{9} \frac{\alpha\alpha_s}{6\pi^2} T^2 e^{-E/T} [\ln(4ET/k_c^2) + C_F] \ , \tag{13}$$

$$E\frac{dR^{\text{annihilation}}}{d^3p} = \frac{5}{9} \frac{\alpha\alpha_s}{3\pi^2} T^2 e^{-E/T} [\ln(4ET/k_c^2) + C_B] \ , \tag{14}$$

where

$$C_F = \frac{1}{2} - C_{\text{Euler}} + \frac{12}{\pi^2} \sum_{n=2}^{\infty} \frac{(-1)^n}{n^2} \ln n = 0.0460... \ , \tag{15}$$

$$C_B = -1 - C_{\text{Euler}} - \frac{6}{\pi^2} \sum_{n=2}^{\infty} \frac{1}{n^2} \ln n = -2.1472... \ . \tag{16}$$

These expressions use the full Fermi-Dirac or Bose-Einstein distribution functions in the final state. Although $E \gg T$, it is not necessarily so that $E_3 \gg T$.

Then one gets slightly different results if one uses the Boltzmann distribution in the final state instead:

$$E\frac{dR^{\text{Compton}}}{d^3p} = \frac{5}{9}\frac{2\alpha\alpha_s}{\pi^4}T^2e^{-E/T} \times[\ln(4ET/k_c^2)+\tfrac{1}{2}-C_{\text{Euler}}]\ , \tag{17}$$

$$E\frac{dR^{\text{annihilation}}}{d^3p} = \frac{5}{9}\frac{2\alpha\alpha_s}{\pi^4}T^2e^{-E/T} \times[\ln(4ET/k_c^2)-1-C_{\text{Euler}}]\ . \tag{18}$$

Corrections to these formulas vanish in the limit $k_c \to 0$.

The essential factors in these rates are easy to understand. There is a factor $\frac{5}{9}$ from the sum of the squares of the electric charges of the u and d quarks, a factor $\alpha\alpha_s$ coming from the topological structure of the diagrams, a factor T^2 from phase space which gives the overall dimension to the rate, a ubiquitous Boltzmann factor $e^{-E/T}$ for photons of energy E, and a logarithm due to the infrared behavior.

These rates agree with those previously reported in the literature [5,12] at least for the dominant logarithmic term. The constant terms are sometimes not given. Or, they may be different if the infrared divergence is regulated by giving the quarks a mass rather than putting a cutoff on the four-momentum transfer.

B. The infrared contribution

The infrared divergence in the photon production rate discussed above is caused by a diverging differential cross section when the momentum transfer goes to zero. Oftentimes long-ranged forces can be screened by many-body effects at finite temperature. Braaten and Pisarski have analyzed problems such as this one in QCD [8]. They have argued that a cure can be found in reordering perturbation theory: by expanding correlation functions in terms of effective propagators and vertices instead of bare ones. These effective propagators and vertices are just the bare ones plus one-loop corrections, with the caveat that the one-loop corrections are evaluated in the high-temperature limit. This makes them relatively simple functions.

For our application we would begin by replacing the bare propagators and vertices in the one-loop diagram of Fig. 1 with effective propagators and vertices. The analysis of Braaten and Pisarski shows that a propagator must be dressed if the momentum flowing through it is soft, where soft means small compared to T. This is because propagation of soft momenta is connected with infrared divergences in loops; if we do not dress these propagators we get infinite answers, so the corrections due to the dressing of the propagators are also infinite and therefore necessary. Thus, the results with soft propagators dressed are really the lowest-order finite results. In our case it is necessary to dress one of the quark propagators because our results diverge otherwise. It is not necessary to dress both, nor is it necessary to dress either of the vertices, because these produce only finite corrections that are of higher order in g. We are thus led to evaluate the diagram shown in Fig. 3. Some insight can be had by expanding the diagram as a power series in g^2. The zeroth-order term reproduces the one-loop diagram of Fig. 1. The order g^2 term reproduces one of the two-loop diagrams of Fig. 1, with the recognition that the quark self-energy is not the exact one-loop self-energy but is approximated by its high-temperature limit. Clearly this is a summation of an infinite set of diagrams that is purposely designed to regulate infrared problems of the type encountered here.

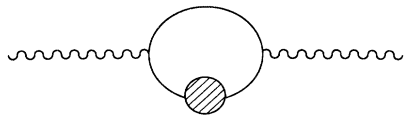

FIG. 3. Braaten-Pisarski dressing of the high-energy photon self-energy.

Starting with Fig. 3, and summing over u and d quarks, we find

$$\Pi^{\mu\nu}(p) = -3\times\frac{5}{9}e^2T\sum_{k_0}\int\frac{d^3k}{(2\pi)^3}\,\text{Tr}[S^*(k)\gamma^\mu S(p-k)\gamma^\nu]\ , \tag{19}$$

where

$$S^*(k) = \frac{1}{D_+(k)}\frac{\gamma_0-\hat{\mathbf{k}}\cdot\boldsymbol{\gamma}}{2} + \frac{1}{D_-(k)}\frac{\gamma_0+\hat{\mathbf{k}}\cdot\boldsymbol{\gamma}}{2} \tag{20}$$

is the dressed propagator for a quark with four-momentum k [13], and

$$S(q) = \frac{1}{d_+(q)}\frac{\gamma_0-\hat{\mathbf{q}}\cdot\boldsymbol{\gamma}}{2} + \frac{1}{d_-(q)}\frac{\gamma_0+\hat{\mathbf{q}}\cdot\boldsymbol{\gamma}}{2} \tag{21}$$

is the bare propagator for a quark with four-momentum $q=p-k$. In these equations

$$D_\pm(k) = -k_0 \pm |\mathbf{k}| + \frac{m_q^2}{|\mathbf{k}|}\left[Q_0\left(\frac{k_0}{|\mathbf{k}|}\right) \mp Q_1\left(\frac{k_0}{|\mathbf{k}|}\right)\right]\ , \tag{22}$$

where Q_0 and Q_1 are the Legendre functions of the second kind, and

$$d_\pm(q) = -q_0 \pm |\mathbf{q}|\ . \tag{23}$$

Using these expressions for the quark propagators, and doing the traces, we obtain

$$\Pi_\mu^{R,\mu}(p) = \frac{10}{3}e^2T\sum_{k_0}\int\frac{d^3k}{(2\pi)^3}\left[\frac{1}{D_+(k)}\left(\frac{1-\hat{\mathbf{k}}\cdot\hat{\mathbf{q}}}{d_+(q)}+\frac{1+\hat{\mathbf{k}}\cdot\hat{\mathbf{q}}}{d_-(q)}\right)+\frac{1}{D_-(k)}\left(\frac{1+\hat{\mathbf{k}}\cdot\hat{\mathbf{q}}}{d_+(q)}+\frac{1-\hat{\mathbf{k}}\cdot\hat{\mathbf{q}}}{d_-(q)}\right)\right]. \tag{24}$$

The retarded self-energy means that p_0 has a small positive imaginary part, as is appropriate in linear response analysis.

We then follow Braaten, Pisarski, and Yuan [14] to compute the imaginary part in the following elegant way:

$$\begin{aligned}\mathrm{Im}\, T\sum_{k_0} F_1(k_0)\, F_2(p_0-k_0) &= \frac{1}{2i}\,\mathrm{Disc}\, T\sum_{k_0} F_1(k_0)\, F_2(p_0-k_0)\\ &= \pi(1-e^{E/T})\int_{-\infty}^{+\infty} d\omega \int_{-\infty}^{+\infty} d\omega'\, f_{\mathrm{FD}}(\omega)\, f_{\mathrm{FD}}(\omega')\,\delta(E-\omega-\omega')\,\rho_1(\omega)\,\rho_2(\omega')\ . \end{aligned} \tag{25}$$

Here f_{FD} is the Fermi-Dirac occupation number and ρ_1 and ρ_2 are the spectral densities for F_1 and F_2. Specifically the latter are related by

$$F(k_0) = \int_{-\infty}^{+\infty} \frac{d\omega}{\omega - k_0 - i\epsilon}\,\rho(\omega). \tag{26}$$

We need the spectral density functions $\rho_\pm$ and $r_\pm$ for the dressed $(1/D_\pm)$ and bare $(1/d_\pm)$ propagators, respectively. They are

$$\rho_\pm(\omega,\mathbf{k}) = \frac{\omega^2-\mathbf{k}^2}{2m_q^2}\left[\delta(\omega-\omega_\pm(|\mathbf{k}|)) + \delta(\omega+\omega_\mp(|\mathbf{k}|))\right] + \beta_\pm(\omega,\mathbf{k})\theta(\mathbf{k}^2-\omega^2)\ , \tag{27}$$

with

$$\beta_\pm(\omega,\mathbf{k}) = \frac{\frac{1}{2}m_q^2(|\mathbf{k}|\mp\omega)}{\left\{|\mathbf{k}|\,(\omega\mp|\mathbf{k}|) - m_q^2\,[Q_0(z)\mp Q_1(z)]\right\}^2 + \left[\frac{1}{2}\pi m_q^2(1\mp z)\right]^2}\ , \tag{28}$$

where $z=\omega/|\mathbf{k}|$, and

$$r_\pm(\omega',\mathbf{q}) = \delta(\omega'\mp|\mathbf{q}|)\ . \tag{29}$$

The $\omega_\pm(|\mathbf{k}|)$ represent the two branches of the dispersion relation for dressed quarks propagating through the plasma. These are determined by setting $D_\pm(\omega,|\mathbf{k}|)=0$ [15]. The plus branch is a monotonically increasing function of momentum; the minus branch has a minimum at nonzero momentum. They have the same effective thermal mass as defined at zero momentum, $\omega_+(0)=\omega_-(0)=m_q=gT/\sqrt{6}$. Both branches always lie within a distance of order gT above the light cone. Putting this information together we obtain

$$\begin{aligned}\mathrm{Im}\,\Pi_\mu^{R,\mu} = &-\frac{10\pi}{3}e^2(e^{E/T}-1)\\ &\times\int\frac{d^3k}{(2\pi)^3}\int_{-\infty}^{+\infty}d\omega\int_{-\infty}^{+\infty}d\omega'\,\delta(E-\omega-\omega')f_{\mathrm{FD}}(\omega)f_{\mathrm{FD}}(\omega')[(1+\hat{\mathbf{q}}\cdot\hat{\mathbf{k}})(\rho_+r_- + \rho_-r_+)\\ &+(1-\hat{\mathbf{q}}\cdot\hat{\mathbf{k}})(\rho_+r_+ + \rho_-r_-)].\end{aligned} \tag{30}$$

In this expression the ρ's are evaluated at $(\omega,\mathbf{k})$ and the r's at $(\omega',\mathbf{q})$.

In the kinetic theory calculation of Sec. II A we were forced to put a cutoff k_c^2 on the four-momentum transfer t (and u) to avoid an infrared divergence. It is only the small piece of phase space left out by Eqs. (11) and (12) that we need to study here. Anything else must necessarily be higher order in g. Inspection of Figs. 2 and 3 shows that the exchanged quark must be dressed and must satisfy

$$-k_c^2 \le \omega^2-\mathbf{k}^2 \le 0. \tag{31}$$

This means that the delta functions (representing poles) in the spectral densities $\rho_\pm$ do not contribute to this order, only the functions $\beta_\pm$ (representing branch cuts).

The energy-conserving delta function, together with the mass-shell delta functions of $r_\pm$, can be used to evaluate the integral over ω' and the integral over the angle between $\mathbf{k}$ and $\mathbf{p}$ in Eq. (30). Then, making use of the inequalities $E\gg T$ and $0\le\mathbf{k}^2-\omega^2\le k_c^2\ll T^2$, we get

$$\mathrm{Im}\,\Pi_\mu^{R,\mu} = -\frac{5e^2}{12\pi}\left(e^{E/T}-1\right)e^{-E/T}\int_0^{k_c}d|\mathbf{k}|\int_{-|\mathbf{k}|}^{|\mathbf{k}|}d\omega\,[(|\mathbf{k}|-\omega)\,\beta_+(\omega,\mathbf{k}) + (|\mathbf{k}|+\omega)\,\beta_-(\omega,\mathbf{k})]\,. \tag{32}$$

The integral involving β_- is the same as the integral involving β_+ so we only need to determine the latter and multiply by 2. Furthermore it is convenient to make the change of variables $|\mathbf{k}|=\tau\cosh\eta$ and $\omega=\tau\sinh\eta$. Then the double integral above becomes

$$2\int_{-\infty}^{+\infty} d\eta \int_0^{k_c} \tau\, d\tau\, (|\mathbf{k}| - \omega)\, \beta_+(\omega, \mathbf{k}) = \frac{m_q^2}{4} \int_{-\infty}^{+\infty} \frac{d\eta}{\cosh^2\eta} \left[\ln\left(\frac{(\Theta + y_c \cosh^2\eta)^2 + 1}{\Theta^2 + 1}\right) - 2\Theta \left[\arctan(\Theta + y_c \cosh^2\eta) - \arctan(\Theta)\right]\right], \quad (33)$$

where

$$\Theta = \frac{2}{\pi} \frac{Q_0(\sinh\eta) - Q_1(\sinh\eta)}{1 - \tanh\eta}, \quad (34)$$

and

$$y_c = \frac{2}{\pi} \frac{k_c^2}{m_q^2}. \quad (35)$$

We still have some freedom in choosing the cutoff k_c. Since g is supposed to be perturbatively small for all of this analysis to make sense let us choose k_c to lie somewhere in the interval

$$m_q \ll k_c \ll T. \quad (36)$$

Then we are allowed to take the limit $y_c \gg 1$ in Eq. (33). Doing so, and dropping terms which vanish in the limit $y_c \to \infty$, we find

$$m_q^2 \ln\left(\frac{k_c^2}{m_q^2}\right) + \frac{m_q^2}{4} \int_{-\infty}^{\infty} \frac{d\eta}{\cosh^2\eta} \left[\ln\left(\frac{4}{\pi^2} \frac{\cosh^4\eta}{\Theta^2 + 1}\right) - 2\Theta\left(\frac{\pi}{2} - \arctan(\Theta)\right)\right]. \quad (37)$$

This remaining integral is a pure number. We have not been able to evaluate it in closed form, but up to the accuracy of our numerical integration (6 significant figures) it is just $-4 \ln 2$.

Now we have all the pieces we need to write down the contribution to the rate coming from the infrared-sensitive part of phase space. Taking Eqs. (1), (32), (33), and (37),

$$E\frac{dR^{\mathrm{BP}}}{d^3p} = \frac{5}{9} \frac{\alpha\alpha_s}{2\pi^2} T^2 e^{-E/T} \ln\left(\frac{k_c^2}{2m_q^2}\right), \quad (38)$$

where

$$2m_q^2 = \tfrac{1}{3} g^2 T^2. \quad (39)$$

This is telling us that in the kinetic theory calculation the effective infrared cutoff is $k_c^2 = 2m_q^2$. In earlier works an infrared cutoff has been imposed by giving the exchanged quark an effective temperature-dependent mass. In Ref. [16] it was taken to be exactly Eq. (39) because the positive branch of the dispersion relation has the asymptotic form at high momentum,

$$\omega_+(k \gg gT) = k + \frac{2m_q^2}{2k} + \cdots, \quad (40)$$

implying an effective mass of $\sqrt{2}m_q$. The negative branch has a dispersion curve which approaches the light cone exponentially at high momentum. Inspection of the spectral densities $\rho_\pm$ shows that its contribution therefore will be exponentially suppressed at typical momenta of order T. In Ref. [5] the infrared cutoff was taken to be $k_c^2 = m_q^2$ because this is the energy of a quark (positive or negative branch) at zero momentum in the plasma. In Ref. [12] many-body effects were not considered at all, and the u and d quarks were given their current-quark masses of 5–7 MeV. The Braaten-Pisarski approach used here includes the full momentum dependence of the dressed quark propagator and gives the precise normalization of the logarithm appearing in the rate.

C. Net rate from hard and soft momentum transfers

Adding the contributions from both the hard momentum transfers, Eqs. (13) and (14), and soft momentum transfers, Eq. (38), we get the net rate

$$E\frac{dR}{d^3p} = \frac{5}{9} \frac{\alpha\alpha_s}{2\pi^2} T^2 e^{-E/T} \ln\left(\frac{2.912}{g^2} \frac{E}{T}\right). \quad (41)$$

This is independent of the cutoff k_c. The Braaten-Pisarski method works beautifully to screen the infrared divergence.

Consider a temperature $T = 200$ MeV. This is approximately the temperature at which one expects the deconfinement and/or chiral-symmetry-restoring phase transition. The value of α_s at this temperature is not known with much certainty, but $\alpha_s = 0.4$ is consistent with a comparison between perturbation theory and lattice gauge simulations [17]. This means that $g^2 = 5$. Whether or not the results obtained here for $g \ll 1$ can be extrapolated to such large values of g is dubious. Perhaps unjustifiably, we think that the results of this section do represent the radiation from QCD plasma to within a factor of 2 or 3 at high photon energy. Anyway we plot the rate Eq. (41) in Fig. 4.

It is apparent that our asymptotic formula breaks down when $E \leq g^2T/2.9$ because the logarithm goes negative. To avoid the assumption that $E \gg T$ we have gone back to the kinetic theory of Sec. II A and evaluated Eq. (4) numerically. We delete the regions $-k_c^2 \leq t \leq 0$

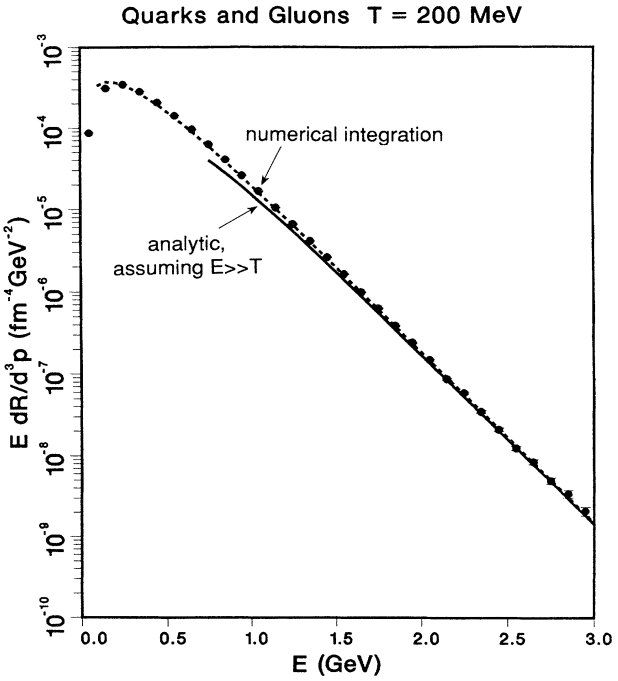

FIG. 4. Thermal production rate of photons in QCD arising from the infrared regulation of Fig. 3 applied to the processes of Fig. 2. The points represent numerical integration of a four-dimensional integral, the solid line is the asymptotic limit ($E >> T$), Eq. (41), and the dashed line modifies that formula by adding 1 to the argument of the logarithm so as to represent the points better for smaller E.

and $-k_c^2 \leq u \leq 0$ for t and u divergences, respectively, with $k_c^2 = g^2T^2/3$. This gives us the "data points" shown in Fig. 4. The error bars represent an estimate of the statistical uncertainty in evaluating the four-dimensional integral. In the same figure we also show an interpolating curve obtained by adding 1 to the argument of the logarithm in Eq. (41). This represents the numerical integration very well for $E > T$. For photon energies less than T we no longer have confidence that our calculation represents the true rate of radiation from QCD plasma for two reasons. First, bremsstrahlung processes were not included and they will certainly be important at low photon energy. Second, the effective cutoff was determined under the assumption that the photon energy was large. If it is not, then all propagators and vertices in Fig. 3 must be dressed. That is outside the scope of this paper.

III. PHOTONS FROM HOT HADRONIC GAS

The thermal emission rate of photons from hot hadronic gas can be treated in a manner analogous to the way we treated QCD plasma in Sec. II. In particular the rate is proportional to the imaginary part of the retarded photon self-energy as given by Eq. (1). If we approximate the self-energy by carrying out a loop expansion to finite order then we reproduce relativistic kinetic theory, as outlined in Eq. (2). The discussion of the first two paragraphs of Sec. II can be repeated because up to that point we did not specify the nature of the strong interactions. It is clear that photons will be emitted from hot hadronic gas because many hadrons are electrically charged and hence couple to the electromagnetic field. In particular π's and ρ mesons are important constituents of such a gas. These mesons will undergo reactions and decays and will occasionally produce photons. As in Sec. II we are interested only in baryon-free matter. Thus nucleons and other more massive baryons will not be considered as relevant and will be ignored in the following analysis: They are simply too heavy to be pair produced with much probability at temperatures of order 200 MeV or less.

In Sec. III A we present some general considerations regarding the production of photons by hadrons. In Sec. III B we compute the differential cross sections for the reactions $hh \rightarrow h\gamma$ where h can be one of the hadrons π, ρ, or η. We focus on these mesons because they are expected to be the most abundant in high-temperature matter as they are in high-energy collisions. We then use these to compute the thermal rate of emission of photons. In Sec. III C we compute the contribution to the emission rate from the decay processes $\rho^0 \rightarrow \pi^+\pi^-\gamma$ and $\omega \rightarrow \pi^0\gamma$. Other decays one may think of are too slow to contribute a significant amount to the thermal rate, although they may contribute a lot to the total yield in a high-energy nucleus-nucleus collision as discussed in Sec. I. Comparison of these results to a QCD plasma is reserved for Sec. IV.

A. General considerations

So far, to our knowledge, there have been no estimates made of the emission rate from hot hadronic gas. At temperatures of the order of the π mass the most important mesonic constituents of the gas will be π's, because they are so light, and ρ mesons, because of their large spin-isospin degeneracy. Furthermore the π-ρ interaction is relatively strong and so it ought to be taken into account. For purposes of illustration let us consider a theory of charged π's interacting with neutral ρ mesons. This is a renormalizable theory so that loop diagrams of all orders make sense.

We couple the neutral rho field ρ_μ and the electromagnetic field A_μ to the pion current. The Lagrangian is

$$\mathcal{L} = |D_\mu \Phi|^2 - m_\pi^2 |\Phi|^2 - \frac{1}{4}\rho_{\mu\nu}\rho^{\mu\nu} + \frac{1}{2}m_\rho^2 \rho_\mu \rho^\mu - \frac{1}{4}F_{\mu\nu}F^{\mu\nu} \tag{42}$$

where $D_\mu = \partial_\mu - ieA_\mu - ig_\rho \rho_\mu$ is the covariant derivative, Φ is the complex pion field, $\rho_{\mu\nu}$ is the rho field-strength tensor and $F_{\mu\nu}$ is the photon field-strength tensor. Following Eq. (1) we want to compute the photon self-energy to order e^2. The diagrammatic expansion is shown in Fig. 5. The one-loop diagrams are of order e^2, the two-loop diagrams of order $e^2 g_\rho^2$. These are the analogues of the QCD diagrams shown in Fig. 1.

Cutting the loop diagrams corresponds to taking the imaginary part or the discontinuity. As usual the one-

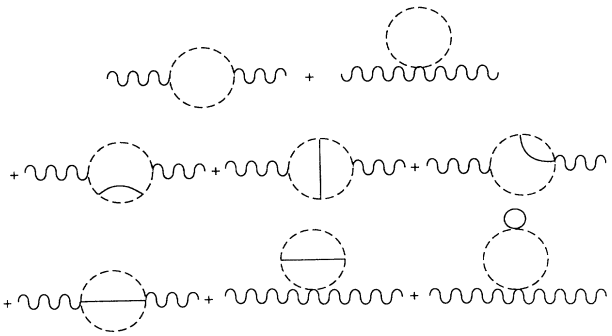

FIG. 5. One- and two-loop contributions to the photon self-energy in a theory of interacting charged pions (dashed lines) and neutral ρ mesons (solid lines).

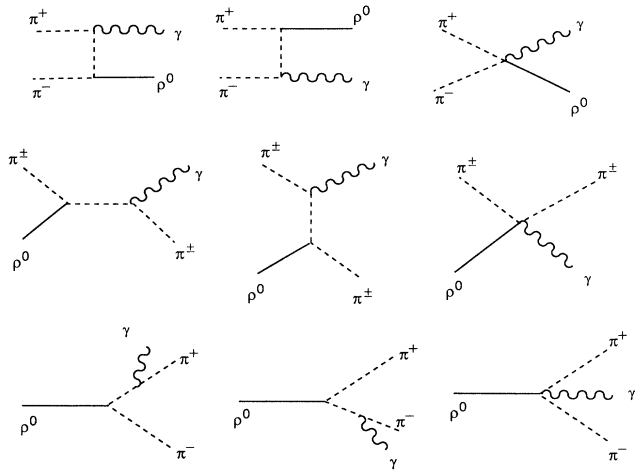

FIG. 6. Photon producing reactions and decays which arise from taking the imaginary parts of the diagrams in Fig. 5.

loop diagrams contribute nothing when the photon is on its mass shell. Imagine cutting the first of the two-loop diagrams in half. We see that this gives one photon, one ρ meson, and two π's as external particles. We insist that the photon be in the final state but the other particles may be in the initial or final states as long as kinematics allows it. The possibilities are $\pi\pi \to \rho\gamma$, $\pi\rho \to \pi\gamma$, $\rho \to \pi\pi\gamma$. Cutting all the two-loop diagrams we end up with the scattering diagrams shown in Fig. 6. There are three categories, the first two of which are analogues of the QCD processes depicted in Fig. 2. The first set is annihilation ($\pi^+\pi^- \to \rho\gamma$), the second is Compton ($\pi^\pm\rho \to \pi^\pm\gamma$), and the third is ρ decay ($\rho \to \pi^+\pi^-\gamma$).

Numerically $g_\rho^2/4\pi = 2.9$ based on the decay rate for $\rho \to \pi\pi$:

$$\Gamma = \frac{g_\rho^2}{48\pi} m_\rho \left(\frac{p_0}{\omega_0}\right)^3 . \tag{43}$$

Here p_0 and ω_0 are the momentum and energy of a π in the rest frame of the ρ. Although one may argue whether this is considered strong or weak coupling, we can make the following observations. Since g_ρ is inferred from experiment one could say that it effectively includes certain higher-order effects such as vertex corrections. Higher-order effects also include the possibility of three-particle collisions to produce a photon plus something else. At low T the density of particles is sufficiently small that two-particle collisions dominate. Finally we remark that order g_ρ^2 corrections to the properties of the ρ meson have been shown to be relatively minor up to temperatures of the order of 150 MeV [11].

B. Hadron collisions

We have calculated the differential cross sections for all annihilation and Compton processes which produce a photon and which involve the mesons $\pi^\pm$, π^0, $\rho^\pm$, ρ^0, and η. We do not take the space in this paper to show all the Feynman diagrams. They are of the generic type discussed in Sec. III A, with the additional complication that charged ρ's can couple to photons. Also the η is supposed to couple predominantly to two ρ mesons, but one of them converts directly to a photon. We have checked that our results are gauge invariant by ensuring that $k_\mu \mathcal{M}^\mu = 0$, where k_μ is the photon momentum and $\mathcal{M}^\mu$ is the sum of amplitudes. The results are

$$\frac{d\sigma}{dt}(\pi^+\pi^- \to \rho^0\gamma) = \frac{\alpha g_\rho^2}{4sp_{\text{c.m.}}^2}\left\{2 - (m_\rho^2 - 4m_\pi^2)\left[\frac{s-2m_\pi^2}{s-m_\rho^2}\left(\frac{1}{t-m_\pi^2}+\frac{1}{u-m_\pi^2}\right)+\frac{m_\pi^2}{(t-m_\pi^2)^2}+\frac{m_\pi^2}{(u-m_\pi^2)^2}\right]\right\} , \tag{44}$$

$$\begin{aligned}\frac{d\sigma}{dt}(\pi^+\pi^0 \to \rho^+\gamma) &= \frac{d\sigma}{dt}(\pi^-\pi^0 \to \rho^-\gamma) \\ &= -\frac{\alpha g_\rho^2}{16sp_{\text{c.m.}}^2}\left[\frac{(s-2m_\rho^2)(t-m_\pi^2)^2}{m_\rho^2(s-m_\rho^2)^2}+\frac{(s-6m_\rho^2)(t-m_\pi^2)}{m_\rho^2(s-m_\rho^2)}+\frac{m_\pi^2}{m_\rho^2}-\frac{9}{2}\right. \\ &\quad \left.+\frac{4(m_\rho^2-4m_\pi^2)s}{(s-m_\rho^2)^2}+\frac{4(m_\rho^2-4m_\pi^2)}{t-m_\pi^2}\left(\frac{s}{s-m_\rho^2}+\frac{m_\pi^2}{t-m_\pi^2}\right)\right] ,\end{aligned} \tag{45}$$

$$\begin{aligned}\frac{d\sigma}{dt}(\pi^+\rho^0 \to \pi^+\gamma) &= \frac{d\sigma}{dt}(\pi^-\rho^0 \to \pi^-\gamma) \\ &= \frac{\alpha g_\rho^2}{12sp_{\text{c.m.}}^2}\left[2-\frac{(m_\rho^2-4m_\pi^2)s}{(s-m_\pi^2)^2}-(m_\rho^2-4m_\pi^2)\left(\frac{s-m_\rho^2+m_\pi^2}{s-m_\pi^2}\frac{1}{u-m_\pi^2}+\frac{m_\pi^2}{(u-m_\pi^2)^2}\right)\right] ,\end{aligned} \tag{46}$$

$$\frac{d\sigma}{dt}(\pi^-\rho^+ \to \pi^0\gamma) = \frac{d\sigma}{dt}(\pi^+\rho^- \to \pi^0\gamma)$$
$$= -\frac{\alpha g_\rho^2}{48 s p_{\rm c.m.}^2}\left\{4(m_\rho^2 - 4m_\pi^2)\left[\frac{u}{(u-m_\pi^2)^2} + \frac{t}{(t-m_\rho^2)^2} - \frac{m_\rho^2}{s-m_\pi^2}\left(\frac{1}{u-m_\pi^2} + \frac{1}{t-m_\rho^2}\right)\right]\right.$$
$$\left. + \left(3 + \frac{s-m_\pi^2}{m_\rho^2}\right)\frac{s-m_\pi^2}{t-m_\rho^2} - \frac{1}{2} + \frac{s}{m_\rho^2} - \left(\frac{s-m_\pi^2}{t-m_\rho^2}\right)^2\right\} \tag{47}$$

$$\frac{d\sigma}{dt}(\pi^0\rho^+ \to \pi^+\gamma) = \frac{d\sigma}{dt}(\pi^0\rho^- \to \pi^-\gamma)$$
$$= \frac{\alpha g_\rho^2}{48 s p_{\rm c.m.}^2}\left[\frac{9}{2} - \frac{s}{m_\rho^2} - \frac{4(m_\rho^2 - 4m_\pi^2)s}{(s-m_\pi^2)^2} + \frac{(s-m_\pi^2)^2 - 4m_\rho^2(m_\rho^2 - 4m_\pi^2)}{(t-m_\rho^2)^2}\right.$$
$$\left. + \frac{1}{t-m_\rho^2}\left(5(s-m_\pi^2) - \frac{(s-m_\pi^2)^2}{m_\rho^2} - \frac{4(m_\rho^2 - 4m_\pi^2)(s - m_\pi^2 + m_\rho^2)}{s-m_\pi^2}\right)\right], \tag{48}$$

$$\frac{d\sigma}{dt}(\pi^+\pi^- \to \eta\gamma) = \frac{\pi\alpha A\,|F_\pi(s)|^2}{16 m_\eta^2 m_\rho^4 s p_{cm}^2}\left[s(u-m_\pi^2)(t-m_\pi^2) - m_\pi^2(s-m_\eta^2)^2\right], \tag{49}$$

$$\frac{d\sigma}{dt}(\pi^+\eta \to \pi^+\gamma) = \frac{d\sigma}{dt}(\pi^-\eta \to \pi^-\gamma) = \frac{\pi\alpha A\,|F_\pi(t)|^2}{16 m_\eta^2 m_\rho^4 s p_{\rm c.m.}^2}\left[t(s-m_\pi^2)(u-m_\pi^2) - m_\pi^2(t-m_\eta^2)^2\right]. \tag{50}$$

In these results we have explicitly verified that crossing symmetry is obeyed. Our notation is that $p_{\rm c.m.}$ is the three-momentum of the colliding particles in their center-of-momentum frame and F_π is the pion electromagnetic form factor [18]. The numerical value of $A = g_{\eta\rho\rho}^2 g_\rho^2/4\pi\gamma_\rho^2 = 4.70 \pm 0.48$ is determined by the full width 1.19 ± 0.12 keV of the eta and the branching ratio $4.88 \pm 0.15\%$ for the decay $\eta \to \pi^+\pi^-\gamma$. For $\pi\pi$ collisions t is the momentum transfer from the π^+ to the γ, or, if there is no π^+ in the initial state then from the π^- to the γ. The $\pi^\pm\pi^0$ reactions have mates where $t \to u$. For $\pi\rho$ or $\pi\eta$ collisions t is the momentum transfer from the ρ or η to the γ. Out of theoretical interest we have also considered the purely electromagnetic annihilation of two pions into two photons:

$$\frac{d\sigma}{dt}(\pi^+\pi^- \to \gamma\gamma)$$
$$= \frac{2\pi\alpha^2}{s p_{\rm c.m.}^2}\left[1 + 2m_\pi^2\left(\frac{1}{t-m_\pi^2} + \frac{1}{u-m_\pi^2}\right)\right.$$
$$\left. + 2m_\pi^4\left(\frac{1}{t-m_\pi^2} + \frac{1}{u-m_\pi^2}\right)^2\right]. \tag{51}$$

For display purposes we have grouped all reactions together into four categories: $\pi\pi \to \rho\gamma$, $\pi\rho \to \pi\gamma$, $\pi\pi \to \eta\gamma$, $\pi\eta \to \pi\gamma$. We have computed the thermal rates for these reactions by inserting the relevant squared amplitudes (proportional to $d\sigma/dt$) into Eq. (3) and carrying out the integration using Monte Carlo techniques. The integrals are four dimensional after using energy-momentum conservation and the isotropy of the gas. The rates at a temperature of 200 MeV are shown in Fig. 7. Reactions involving the rho meson are clearly the dominant ones, as expected. The rate at low photon energy is dominated by reactions with the rho in the final state, because these reactions are endothermic with most of the available energy going into the rho mass [19]. At high photon energy reactions with the rho in the initial state are dominant because these reactions are

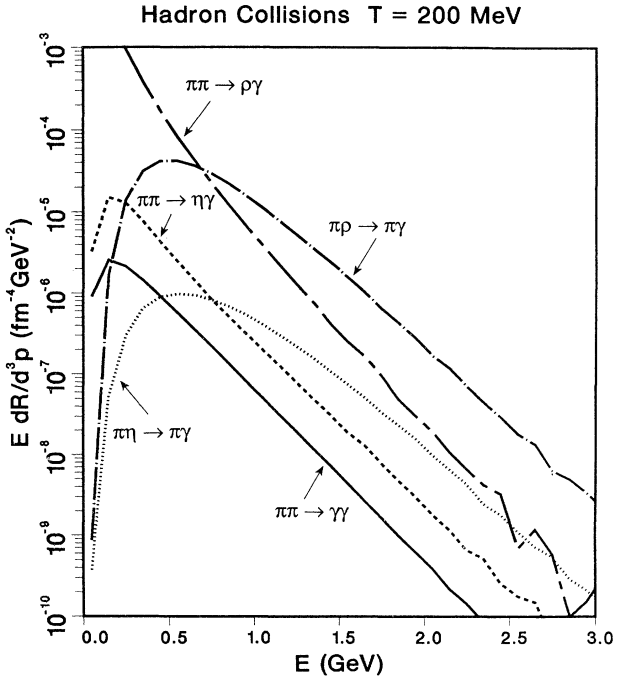

FIG. 7. The thermal rate for various photon producing hadron reactions.

exothermic; most of the rho mass is available for producing high-energy photons. Similar remarks can be made concerning reactions involving the η meson, but because the η coupling constant is much smaller so are the rates. One could imagine other mesons contributing via two-body reactions, such as the ω, but they all have coupling constants much smaller than the ρ's. We do not consider them here. Finally we show the rate from pion annihilation into two photons. This reaction is negligible compared to those involving the rho. For those wishing to peek ahead, notice that the scale of Fig. 7 is identical to that of Fig. 4.

C. Vector-meson decays

As we saw in Sec. III A there can be contributions to the thermal photon yield from the decay of mesons in matter. One such decay is $\rho^0 \rightarrow \pi^+\pi^-\gamma$. Another is $\omega \rightarrow \pi^0\gamma$, which corresponds to a one-loop contribution to the photon self-energy. In high-energy hadron collisions, important contributors to photons of moderate energy are the final-state electromagnetic decays $\pi^0 \rightarrow \gamma\gamma$ and $\eta \rightarrow \gamma\gamma$. But these decay rates are too small to compete with those processes listed above at finite temperature.

Let us first consider ω decay as it is the simpler one. In the ω rest frame the invariant momentum distribution of the photon is

$$E\frac{dN}{d^3p} = \frac{\delta(E-E_0)}{4\pi E_0} , \tag{52}$$

where E_0 is the photon energy in this frame. We now must give the ω a thermal momentum distribution. Folding it with the photon distribution in the ω rest frame, multiplying by the width of the ω and by the pion Bose-Einstein enhancement factor, we get the photon distribution in the rest frame of the gas:

$$E\frac{dR_{\omega\rightarrow\pi^0\gamma}}{d^3p} = \frac{\Gamma_{\omega\rightarrow\pi^0\gamma}}{4\pi E_0}\frac{3}{(2\pi)^3} \times \int d^3p_\omega\, \delta\left(\frac{E_\omega E - \mathbf{p}_\omega\cdot\mathbf{p}}{m_\omega} - E_0\right) \times f_{\rm BE}(E_\omega)[1+f_{\rm BE}(E_\omega - E)] . \tag{53}$$

Integrating over the angles we are left with a one-dimensional integral which must be evaluated numerically:

$$E\frac{dR_{\omega\rightarrow\pi^0\gamma}}{d^3p} = \frac{3m_\omega\Gamma_{\omega\rightarrow\pi^0\gamma}}{16\pi^3E_0E}\int_{E_{\rm min}}^{\infty} dE_\omega\, E_\omega f_{\rm BE}(E_\omega) \times[1+f_{\rm BE}(E_\omega - E)] , \tag{54}$$

where $E_{\rm min} = m_\omega(E^2+E_0^2)/2EE_0$. We can get a good idea of the behavior of this distribution by neglecting the Bose-Einstein enhancement and by approximating the ω distribution by a relativistic Boltzmann distribution function:

$$E\frac{dR}{d^3p} = \frac{3m_\omega T(E_{\rm min}+T)}{16\pi^3E_0E}\Gamma_{\omega\rightarrow\pi^0\gamma}\, e^{-E_{\rm min}/T} . \tag{55}$$

This distribution goes to zero as $E \rightarrow 0$ and as $E \rightarrow \infty$. The full expression, Eq. (54), is plotted in Fig. 8.

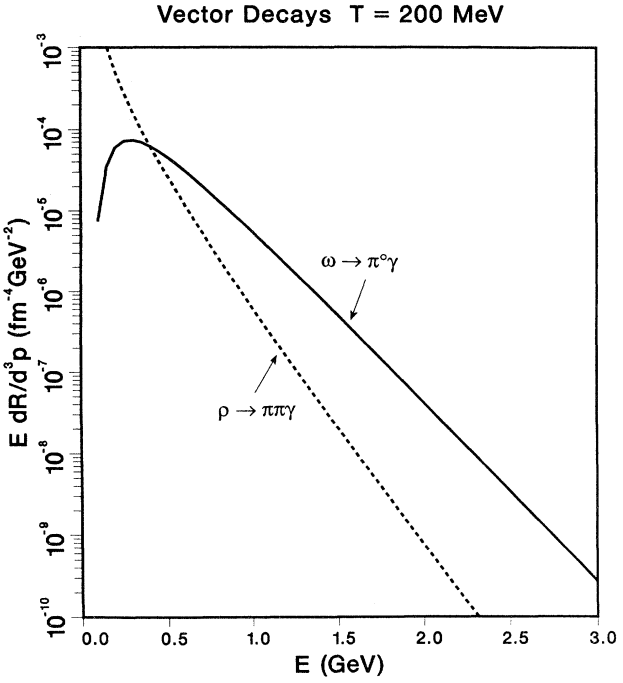

FIG. 8. The thermal rate for several photon producing vector-meson decays.

The decay of the ρ is a little more complicated since it gives rise to a three-body final state. The invariant decay rate distribution is [20]

$$\hat{\Gamma}(E) = E\frac{d\Gamma_{\rho\rightarrow\pi\pi\gamma}}{d^3p} = \frac{\alpha g_\rho^2}{24\pi^3 m_\rho}\left\{\left(1-\frac{4m_\pi^2}{s}\right)^{1/2} - \frac{m_\rho^2-4m_\pi^2}{m_\rho E}\left[\frac{s-2m_\pi^2}{s-m_\rho^2}\ln\left(\frac{\sqrt{s}+\sqrt{s-4m_\pi^2}}{2m_\pi}\right) + \frac{\sqrt{s(s-4m_\pi^2)}}{4m_\rho E}\right]\right\} . \tag{56}$$

Here $s = (p_+ + p_-)^2 = m_\rho(m_\rho - 2E)$ is the square of the energy of the 2π system in the π-π rest frame. Folding this distribution with the thermal ρ momentum distribution we have

$$E\frac{dR_{\rho\rightarrow\pi\pi\gamma}}{d^3p} = \frac{3}{(2\pi)^3}\int \hat{\Gamma}\left(E' = \frac{EE_\rho - \mathbf{p}\cdot\mathbf{p}_\rho}{m_\rho}\right) \times f_{\rm BE}(E_\rho)d^3p_\rho . \tag{57}$$

The integration over the angle ϕ can be done trivially but a two-dimensional integration remains, to be done numerically. Actually the astute reader will notice that this expression does not include the Bose-Einstein enhancement of the final-state pions. The reason is that the decay distribution of Eq. (56) already has integrated out the pion degrees of freedom. Rather than put the pions back in and integrate over the full three-body final state, we have inserted the minimal Bose-Einstein enhancement by sharing the energy $E_\rho - E$ equally between the pions. Unequal sharing increases the enhancement, so we multiply the integrand by $\{1 + f_{\rm BE}[\frac{1}{2}(E_\rho - E)]\}^2$.

Numerical results are shown in Fig. 8. The difference between ρ and ω decays is plain to see. The ω decay dominates at high energy because its final state is two-body. The ρ decay dominates at low energy because its final state is three-body. In fact ρ decay occurs even in the absence of an associated photon, so it is no surprise that the rate increases with decreasing energy. Concerning the Bose-Einstein enhancement, we have found that including it minimally increases the yield by about 20%. So including it exactly would increase the yield by some percent more.

In recent years the decay mode $\rho^0 \to \pi^+\pi^-\gamma$ has been measured [21]. Its branching ratio is $(1.10 \pm 0.14)\%$ for photons above 50 MeV. This is in agreement with Eq. (56).

IV. QUARK-GLUON PLASMA vs HADRONIC GAS

In Secs. II and III we calculated the thermal production rates for high-energy ($E > 3T$) photons from baryon-free quark-gluon plasma and from a gas of π, η, ρ, and ω mesons. In this section we compare these two rates and discuss possible experimental ramifications.

We begin with our surprising result. The photon production rates at $T = 200$ MeV are shown in Fig. 9. The most obvious feature is that the quark-gluon plasma and the hadron gas produce photons with energies from 1 to 3 GeV at the same rate. Not only is the shape of the production curve the same but the overall magnitude is too. The hadron gas shines just as brightly as the quark-gluon plasma.

The conclusion is that high-energy photons make a good "thermometer" for the hot matter created in high-energy collisions. The thermal production rate depends only on the temperature, so any temperature deduced from the thermally produced photons is nearly independent of assumptions about the phase of the matter. If we know the temperature and volume of the system as functions of time then

$$E\frac{dN}{d^3p} = \int dt\, V(t)\, E\frac{dR}{d^3p}(\mathrm{p}, T(t)). \tag{58}$$

The momentum distribution of the photons is equal to the thermal production rate integrated over space-time. Conversely, based on these results it does not seem likely that high-energy photons will distinguish between quark-gluon plasma and hot hadronic gas.

If QCD undergoes a strong first-order phase transition then the created matter is expected to remain for a long time at the transition temperature T_c [22], and consequently most thermally produced photons will come from matter at temperature T_c. This would allow us to determine T_c.

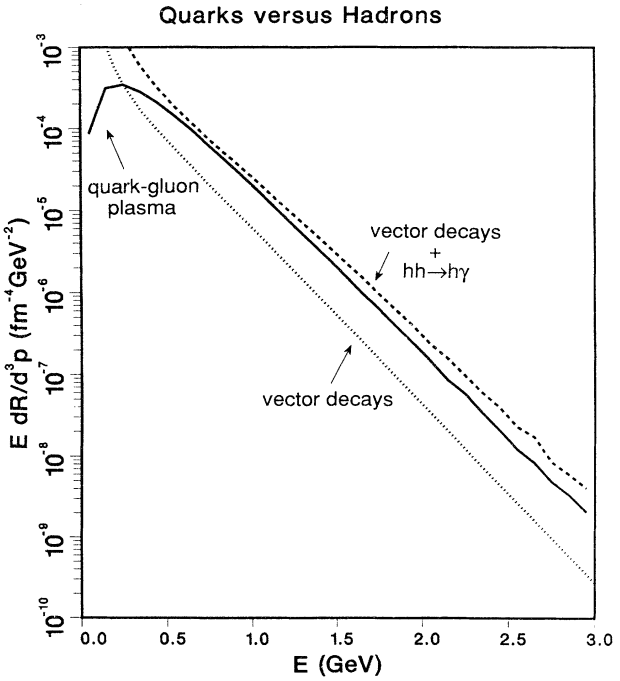

FIG. 9. Comparison among photon production from a quark-gluon plasma, from vector-meson decay, and from vector-meson decay plus hadron reactions, all at the same temperature of 200 MeV.

For illustration, consider photon production in Pb-Pb collisions at 100 GeV per nucleon in the center-of-mass frame, conditions expected at RHIC. In a central collision the cross-sectional area of created hot matter, σ, is approximately 100 fm^2. The temperature at time $t = 1$ fm/c, T_0, is estimated to be at least 250–300 MeV. Ignoring transverse expansion of the hot matter the volume at time t is

$$V(t) = \sigma t. \tag{59}$$

The matter reaches the phase transition temperature T_c at the time

$$t_1 = (T_0/T_c)^3\ \mathrm{fm}/c, \tag{60}$$

and remains at T_c until the time

$$t_2 = rt_1, \tag{61}$$

where r is the ratio of the number of degrees of freedom of quark-gluon plasma to hadron gas. Typically r is taken to be about 10.

Using the conservative estimate of $T_0 = 250$ MeV, and $T_c = 200$ MeV, we find that the energy radiated as photons in the interval from 1 to 3 GeV is about 0.4 GeV per collision. This falls to 0.25 GeV if $T_c = 170$ MeV instead. If we take $T_0 = 300$ MeV the energy radiated is a factor 3

larger in both cases. The rate falls off very quickly with energy so most of these photons will have energies near 1 GeV, and the number of emitted photons is estimated to be from 0.1 to 1 per collision for this parameter range.

Looking at Fig. 9 again we see that the rate falls by roughly a factor 10^4 from 1 to 3 GeV. We estimate at least 1 photon with $E > 1$ GeV per 10 collisions, so we expect to see at least 1 photon with $E > 3$ GeV every 10^5 collisions. Therefore, if thermally produced photons can be extracted experimentally from 10^7 collisions, we will obtain the thermal production rate from 1 to 3 GeV with a statistical error of less than 0.1% at 1 GeV and 10% at 3 GeV.

These experimental uncertainties are much smaller than the theoretical ones in current calculations. However, this level of experimental accuracy would not be wasted. Although we cannot claim to know the absolute yield to even within a factor of 2, the relationship between the exponential falloff and T_c seems quite firm, and if this exponential decrease is measured experimentally it will provide a very good determination of T_c. Even a pessimistic estimate of 100% error in the rate at 3 GeV results in only about a 10% error in the estimate of T_c.

The main experimental difficulty will be the extraction of the thermally produced photons from the background [23,24]. There will be a large background of photons coming from final-state π^0 and η decays that must be removed from the data. There may also be a substantial background from high-energy photons produced in jets.

It is interesting to figure out how long it would take photons to come to equilibrium with the strongly interacting particles. Using detailed balance, and ignoring expansion of the matter, the photon number distribution in six-dimensional phase space ($dn/d^3p = dN/d^3x\,d^3p$) satisfies the rate equation

$$\frac{d}{dt}\left(\frac{dn}{d^3p}\right) = \frac{dR}{d^3p}\left(1 - \frac{dn/d^3p}{dn_{\rm eq}/d^3p}\right). \tag{62}$$

The equilibrium distribution is just the Planck distribution

$$\frac{dn^{\rm eq}}{d^3p} = \frac{2}{(2\pi)^3}\frac{1}{e^{E/T}-1}. \tag{63}$$

Starting with no photons at $t = 0$, the solution to the rate equation (at fixed temperature) is

$$\frac{dn}{d^3p} = \frac{dn^{\rm eq}}{d^3p}\left(1 - e^{-t/\tau}\right) \tag{64}$$

where the equilibration time is

$$\tau = \frac{dn^{\rm eq}/d^3p}{dR/d^3p}. \tag{65}$$

Recalling Eq. (41), and modifying the logarithm so as to represent better the rate for all $E > 2T$, we obtain

$$\tau = \frac{9E}{10\pi\alpha\alpha_s T^2}\frac{1}{\ln\left(\frac{2.9}{g^2}\frac{E}{T}+1\right)}. \tag{66}$$

At $T = 200$ MeV this is 270, 356, 505, and 639 fm/c for $E = 0.5$, 1, 2 and 3 GeV, respectively. Thus high-energy photons will not be anywhere near equilibrium in high-energy nuclear collisions, as stated in the Introduction. The same conclusion applies in the hadronic phase since production rates are comparable. These times also give us the mean free paths. We point out that these are large compared to the size of the system, so that high-energy photons will escape from the system without interaction.

V. FORM FACTORS

In Sec. III we studied photon production by hadrons. The interactions were modeled by local relativistic quantum field theory. We know that hadrons are composite objects, so they may need form factors at high-momentum transfer. How much will form factors influence our results? Form factors are a very delicate subject, especially when electromagnetism and its gauge invariance are involved. We restrict our attention to the reaction $\pi^+\pi^- \to \rho^0\gamma$. This reaction provides a good testing ground for the importance of form factors because the incoming pions must provide the energy necessary to create the heavy ρ meson plus a high momentum photon. Also the interaction is renormalizable so perhaps it makes sense to think of the form factors as arising from higher-order effects.

The most general form of the $\pi\pi\gamma$ vertex is shown in Fig. 10. It involves two scalar functions, h_+ and h_-, that depend on the three invariants p_i^2, p_f^2, and k^2 [25]:

$$\Gamma^\mu(p_i,p_f,k) = (p_i+p_f)^\mu h_+(p_i^2,p_f^2,k^2) + (p_i-p_f)^\mu h_-(p_i^2,p_f^2,k^2)\ . \tag{67}$$

This vertex is related to the dressed pion propagator Δ by the Ward-Takahashi identity [26]:

$$(p_i-p_f)_\mu\Gamma^\mu(p_i,p_f,k) = \Delta^{-1}(p_i) - \Delta^{-1}(p_f)\ . \tag{68}$$

For both pion lines on mass shell h_- must vanish and $h_+(m_\pi^2,m_\pi^2,k^2) = F_\pi(k^2)$ is the pion electromagnetic form factor. For simplicity we assume $h_- = 0$ for all momentum configurations. This is not necessarily true but it suffices to get an estimate of the importance of form factors. For our calculations we need only h_+ when one pion is off mass shell while both the other pion and the photon are on mass shell. Given the function $h_+(p^2,m_\pi^2,0)$, the pion propagator is determined by the Ward-Takahashi identity (68):

$$\Delta(p) = \frac{1}{p^2-m_\pi^2}\frac{1}{h_+(p^2,m_\pi^2,0)}\ . \tag{69}$$

Next we need the $\pi\pi\rho\gamma$ vertex, shown in Fig. 11. Its

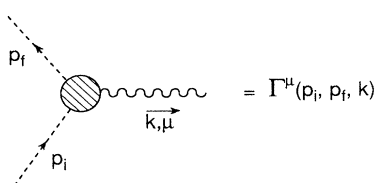

FIG. 10. The $\pi\pi\gamma$ vertex.

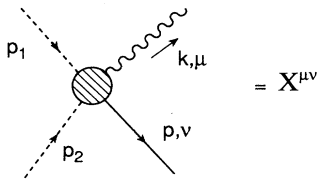

FIG. 11. The $\pi\pi\rho\gamma$ vertex.

general form can be taken to be

$$X^{\mu\nu} = ag^{\mu\nu} + b(p_1^\mu p_2^\nu + p_1^\nu p_2^\mu) + c(p_1^\mu p_1^\nu + p_2^\mu p_2^\nu) + dp^\mu k^\nu . \tag{70}$$

We do not include terms proportional to k^μ because the photon is on mass-shell so that the photon polarization ϵ_μ is transverse ($\epsilon_\mu k^\mu = 0$). When we compute amplitudes, $X^{\mu\nu}$ is contracted with ϵ_μ so these terms vanish.

The amplitude for $\pi^+\pi^- \to \rho^0\gamma$ is $\mathcal{M}^{\mu\nu} = \mathcal{M}_1^{\mu\nu} + \mathcal{M}_2^{\mu\nu} + X^{\mu\nu}$, where $\mathcal{M}_1^{\mu\nu}$ and $\mathcal{M}_2^{\mu\nu}$ are given in Fig. 12 and are evaluated to be

$$\mathcal{M}_1^{\mu\nu} = \frac{h_+(q^2)}{q^2 - m_\pi^2}(p_2 - q)^\mu (p_1 + q)^\nu , \tag{71}$$

$$\mathcal{M}_2^{\mu\nu} = \frac{h_+(q'^2)}{q'^2 - m_\pi^2}(p_1 + q')^\mu (p_2 - q')^\nu , \tag{72}$$

$$q = k - p_2 = p_1 - p, \quad q' = p - p_2 = p_1 - k. \tag{73}$$

Here we assume that $h_+(p^2, m_\pi^2, k^2 = 0) = h_+(p^2, m_\pi^2, k^2 = m_\rho^2)$. This is not true in general, but it is true whenever the $\pi\pi\gamma$ and $\pi\pi\rho$ form factors are

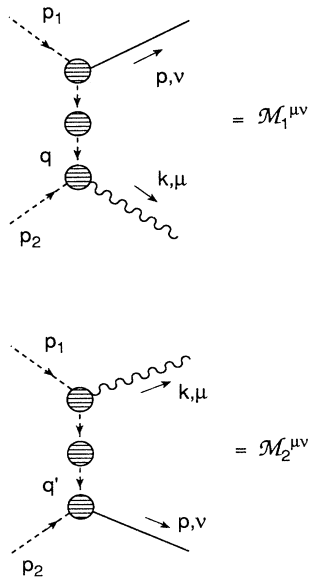

FIG. 12. Two amplitudes contributing to the reaction $\pi^+\pi^- \to \rho^0\gamma$ including dressing of the vertices and the exchanged pion.

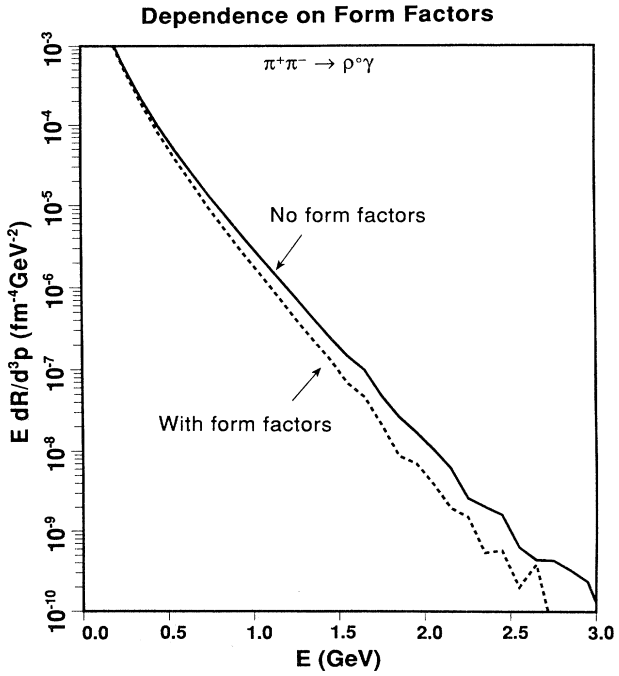

FIG. 13. Influence of the monopole form factors chosen in the text on the thermal production rate for $\pi^+\pi^- \to \rho^0\gamma$.

equal. Gauge invariance requires that $k_\mu \mathcal{M}^{\mu\nu} = 0$. This constrains the functions a, b, c, and d if h_+ is considered as given. For simplicity we assume that $d = 0$, obtaining

$$a = h_+(q^2) + h_+(q'^2) \tag{74}$$

and

$$b = -c = \frac{h_+(q'^2) - h_+(q^2)}{k \cdot (q + q')} . \tag{75}$$

Thus the $\pi\pi\rho\gamma$ vertex has the form

$$X^{\mu\nu} = ag^{\mu\nu} - b(p_1 - p_2)^\mu (p_1 - p_2)^\nu . \tag{76}$$

Finally, for definiteness, we take h_+ to be a monopole with m_ρ as the cutoff mass:

$$h_+(q^2) = \frac{m_\rho^2 - m_\pi^2}{m_\rho^2 - q^2} . \tag{77}$$

With the form factors as constructed above we have computed $d\sigma/dt$ with the help of the algebraic manipulator REDUCE. (The final expression is too lengthy to present here.) Then the thermal rate was computed just as in Sec. III. The result is shown in Fig. 13. We observe that the form factors become increasingly important as the photon energy increases, as expected. However, the effect is not so great: at photon energies of order 2–2.5 GeV the suppression is only about a factor of 2.8. The explanation is that $d\sigma/dt$ is peaked at $t = 0$ and at $u = 0$. [See Eq. (44).] If all hadron reactions were suppressed by the same amount as shown in Fig. 13, we would conclude from Fig. 8 that the quark and hadron curves would lie even closer to each other.

VI. SUMMARY

In Sec. II we calculated the thermal production rate for high-energy ($E \gg T$) photons from baryon-free quark-gluon plasma, including all terms up to first order in α and α_s. We removed the divergences from this rate by using the thermal propagator approach of Braaten and Pisarski. In Sec. III we calculated the same rate for a gas of π, ρ, ω and η mesons. This was done to effectively the same order as for a quark-gluon plasma, both of them arising from two-loop contributions to the photon self-energy at finite temperature.

In Sec. IV we showed that the production rate for high-energy photons from hot, strongly-interacting matter is, within theoretical uncertainties, independent of the phase of that matter. This conclusion is based on our numerical results at $T = 200$ MeV. By continuity it must be true for nearby temperatures too. Consequently, if the thermally produced photon component can be extracted from the background, it will provide an excellent thermometer for ultrarelativistic nuclear collisions. Conversely high momentum photons would not seem to distinguish between a quark-gluon plasma and hadron gas. Finally, in Sec. V we estimated the effect of form factors on our hadron gas calculation, concluding that they give only relatively small changes in the photon production rate for $E < 3$ GeV.

Further work is clearly justified by our results. Theoretically a more complete analysis of strong and electromagnetic form factors of mesons at finite temperature would be useful. We should also consider the inclusion of heavier mesons such as the a_1 [27] as well as the kaons and other strange mesons. Then the microscopic cross sections or rates for photon production should be used in dynamical models of nuclear collisions to predict absolute yields. The simple estimates made in Sec. IV suggest that if QCD exhibits a first-order phase transition the experimental measurement of high-energy photons should allow an accurate determination of T_c.

ACKNOWLEDGMENTS

This study was motivated by discussions J.K. had with R. Pisarski and H. Gutbrod. J.K. thanks R. Pisarski and E. Braaten for helpful conversations concerning the QCD infrared regulation technique, and L. McLerran for remarks on the significance of form factors. D.S. thanks the Department of Physics of the University of Jyväskylä for their hospitality (and computer time) while this manuscript was being written. P.L. thanks the Theoretical Physics Institute at the University of Minnesota for support and hospitality during his visit. This research was supported by the U.S. Department of Energy under Contract No. DOE/DE-FG02-87ER-40328; computer facilities were provided by the Minnesota Supercomputer Institute.

* Permanent address: Department of Theoretical Physics, Comenius University, CS-842 15 Bratislava, Czechoslovakia.

† Present address: Physics Dept., Kent State University, Kent, OH 44242.

[1] E. V. Shuryak, Yad. Fiz. **28**, 796 (1978) [Sov. J. Nucl. Phys. **28**, 408 (1978)].

[2] K. Kajantie and H. I. Miettinen, Z. Phys. C **9**, 341 (1981).

[3] F. Halzen and H. C. Liu, Phys. Rev. D **25**, 1842 (1982).

[4] B. Sinha, Phys. Lett. **128B**, 91 (1983).

[5] R. C. Hwa and K. Kajantie, Phys. Rev. D **32**, 1109 (1985).

[6] G. Staadt, W. Greiner, and J. Rafelski, Phys. Rev. D **33**, 66 (1986).

[7] V. Cerny, P. Lichard, and J. Pisut, Z. Phys. C **31**, 163 (1986).

[8] R. D. Pisarski, Nucl. Phys. **B309**, 476 (1988); Phys. Rev. Lett. **63**, 1129 (1989); E. Braaten and R.D. Pisarski, Nucl. Phys. **B337**, 569 (1990).

[9] H. A. Weldon, Phys. Rev. D **28**, 2007 (1983).

[10] L. D. McLerran and T. Toimela, Phys. Rev. D **31**, 545 (1985).

[11] C. Gale and J. I. Kapusta, Nucl. Phys. **B357**, 65 (1991).

[12] M. Neubert, Z. Phys. C **42**, 231 (1989).

[13] It is usually stated that the high-temperature approximation as applied to the quark self-energy is valid when both the energy and the three-momentum are small compared to T. In fact it is less restrictive. It only requires that we are close to the light cone, $|k^2| \ll T^2$. This can be seen by inspection of Appendix A of H. A. Weldon, Phys. Rev. D **26**, 2789 (1982). This is fortunate tor otherwise the Braaten-Pisarski resummation technique would not suffice to screen the infrared divergence encountered here.

[14] E. Braaten, R.D. Pisarski, and T.C. Yuan, Phys. Rev. Lett. **64**, 2242 (1990).

[15] V. V. Klimov, Yad. Fiz. **33**, 1734 (1981) [Sov. J. Nucl. Phys. **33**, 934 (1981)].

[16] K. Kajantie and P. V. Ruuskanen, Phys. Lett. **121B**, 352 (1983).

[17] J. I. Kapusta, *Finite Temperature Field Theory* (Cambridge University Press, Cambridge, England, 1989).

[18] G. J. Gounaris and J. J. Sakurai, Phys. Rev. Lett. **21**, 244 (1968).

[19] For the $\pi\pi \to \rho$ (or η) γ reactions we had to impose a lower cutoff on the photon energy as measured in the $\pi\pi$ rest frame in order to avoid a divergence in the cross sections as the photon energy approached zero. Rigorous regulation of this divergence depends on higher-order QED effects: the effective expansion parameter is actually $\alpha \ln(E_\pi/E_\gamma)$, not α. We found that deleting photons with energy $E_\gamma < E_\pi/5.5$ (in $\pi\pi$ rest frame) affected the thermal rate only for $E < 0.3$ GeV (in thermal rest frame). Therefore our results are not reliable for low photon energies.

[20] P. Singer, Phys. Rev. **130**, 2441 (1963); **161**, 1694 (1967).

[21] I. B. Vasserman *et al.*, Yad. Fiz. **47**, 1635 (1988) [Sov. J. Nucl. Phys. **47**, 1035 (1988)].

[22] J. D. Bjorken, Phys. Rev. D **27**, 140 (1983).

[23] P. V. Ruuskanen, in *Proceedings of the ECFA Large*

Hadron Collider Workshop, Aachen, Germany, 1990, edited by G. Jarlskog and D. Rein (CERN Report No. 90-10, Geneva, Switzerland, 1990), Vol. II, p. 1164.
[24] WA80 Collaboration, R. Albrecht *et al.*, Z. Phys. C **51**, 1 (1991).
[25] H. W. L. Naus and J. H. Koch, Phys. Rev. C **39**, 1907 (1989).
[26] J. C. Ward, Phys. Rev. **78**, 182 (1950); Y. Takahashi, Nuovo Cimento **6**, 371 (1957).
[27] E. Shuryak (private communication).